The Journal of Chemical Physics

Shape-controlling effects of hydrohalic and carboxylic acids in TiO_2 nanoparticle synthesis

Cite as: J. Chem. Phys. **152**, 064702 (2020); https://doi.org/10.1063/1.5138717
Submitted: 15 November 2019 . Accepted: 19 January 2020 . Published Online: 10 February 2020

K. Sellschopp, W. Heckel, J. Gäding, C. J. Schröter, A. Hensel, T. Vossmeyer, H. Weller, S. Müller, and G. B. Vonbun-Feldbauer

The Journal of Chemical Physics ARTICLE scitation.org/journal/jcp

Shape-controlling effects of hydrohalic and carboxylic acids in TiO_2 nanoparticle synthesis

Cite as: J. Chem. Phys. 152, 064702 (2020); doi: 10.1063/1.5138717
Submitted: 15 November 2019 • Accepted: 19 January 2020 •
Published Online: 10 February 2020

K. Sellschopp,[1] W. Heckel,[1] J. Gäding,[1] C. J. Schröter,[2] A. Hensel,[2] T. Vossmeyer,[2] H. Weller,[2] S. Müller,[1] and G. B. Vonbun-Feldbauer[1,a)]

AFFILIATIONS

[1]Institute of Advanced Ceramics, Hamburg University of Technology, Denickestr. 15, 21073 Hamburg, Germany
[2]Institute of Physical Chemistry, University of Hamburg, Grindelallee 117, 20146 Hamburg, Germany

Note: This paper is part of the JCP Special Topic on Oxide Chemistry and Catalysis.
[a)]**Author to whom correspondence should be addressed:** gregor.feldbauer@tuhh.de

ABSTRACT

The ability to synthesize nanoparticles (NPs), here TiO_2, of different shapes in a controlled and reproducible way is of high significance for a wide range of fields including catalysis and materials design. Different NP shapes exhibit variations of emerging facets, and processes such as adsorption, diffusion, and catalytic activity are, in general, facet sensitive. Therefore, NP properties, e.g., the reactivity of NPs or the stability of assembled NPs, depend on their shape. We combine computational modeling based on density functional theory with experimental techniques such as transmission electron microscopy, energy-dispersive x-ray spectroscopy, and x-ray powder diffraction to investigate the ability of various adsorbates, including hydrohalic and carboxylic acids, to influence NP shape. This approach allows us to identify mechanisms stabilizing specific surface facets and thus to predict NP shapes using computational model systems and to experimentally characterize the synthesized NPs in detail. Shape-controlled anatase TiO_2 NPs are synthesized here in agreement with the calculations in platelet and bi-pyramidal shapes by employing different precursors. The importance of the physical conditions and chemical environment during synthesis, e.g., via competitive adsorption or changes in the chemical potentials, is studied via *ab initio* thermodynamics, which allows us to set previous and new results in a broader context and to highlight potentials for additional synthesis routes and NP shapes.

I. INTRODUCTION

Titania (TiO_2) nanoparticles (NPs) are commercially available and used in applications ranging from pigments in sunscreen and other cosmetic products to catalysis.[1] Because of its bandgap, abundance, stability, and low toxicity, TiO_2 is especially attractive for photocatalysis, photovoltaics, and batteries.[2,3] A recent study even showed that TiO_2 NPs can be used as support for Pt atoms in the emerging field of single atom catalysis.[4] Furthermore, TiO_2 NPs can be assembled in a three-dimensional structure to form hybrid materials with extraordinary mechanical strength[5,6] and adjustable elasticity.[7] Most of these applications depend on the interaction of TiO_2 surfaces with the surrounding medium and certain types of functional chemical groups. The reactivity in (photo-)catalysis and the binding strength of the different adsorbates change according to the underlying crystal facet of the TiO_2 NPs. As illustrated in Fig. 1, the total surface areas of individual facets vary with the shape of the NPs. Therefore, shape-control during the synthesis of TiO_2 NPs is of crucial importance.

Experimentally, several aqueous and non-aqueous synthesis routes are known to produce TiO_2 NPs.[8–12] Even though the rutile structure has the lowest bulk formation enthalpy,[13] NPs are usually formed in the anatase structure due to the lower surface enthalpy compared to rutile.[14–16] Addition of fluoride during synthesis is

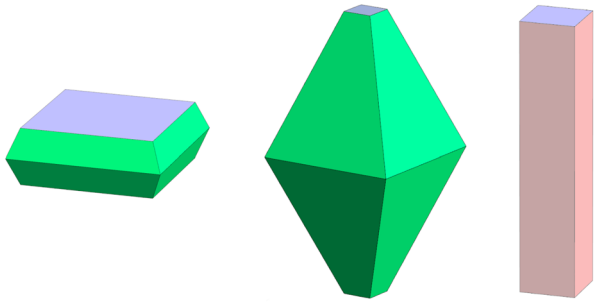

FIG. 1. Typical shapes of anatase TiO_2 nanoparticles. From left to right: platelet dominated by {001} facets (blue), bipyramid dominated by {101} facets (green), and rod dominated by {100} facets (red).

known to produce platelet-shaped particles[17] dominated by {001} facets, whereas chloride can stabilize bi-pyramidal particles with an increased area of the {101} facets or even cuboids, showing the {100} and {001} facets when combined with fluoride.[18] In non-aqueous synthesis, carboxylic acids are used to provide the oxygen needed for TiO_2 synthesis. Rod-shaped particles can then be produced by adding amines to the solution.[11] A fundamental understanding of these shape-control processes from theory, however, only exists for the influence of fluoride. Initially, fluoride adsorption was thought to stabilize the {001} facet.[17] However, more thorough calculations showed that a substitution of surface hydroxyl groups by fluoride is the cause of this stabilization.[19,20] To the best of the authors' knowledge, studies on the substitution of surface hydroxyl groups by other halides (Cl, Br, and I) have not been reported in the literature so far.

In non-aqueous synthesis, the halides adsorbed on the TiO_2 surfaces are thought to be replaced by carboxylic acid adsorbates. Hence, the final particle is also functionalized with carboxylic acids. However, with strong binding halides at the surface and possible substitution structures, the question arises, which ligands dominate in this competitive adsorption process and how this influences the shape of the resulting NPs?

Here, the adsorption of the hydrohalic acids (HF, HCl, HBr, and HI) and carboxylic acids (acetic acid and benzoic acid) on anatase TiO_2 (001), (100), and (101) surfaces are studied with density functional theory (DFT) calculations. For the (001) surface, both the unreconstructed 1 × 1 surface and the well-known 1 × 4 reconstruction[21] are considered. Acetic and benzoic acids are studied to represent larger molecules used in non-aqueous synthesis while at the same time reducing the computational cost of the calculations. Acetic acid is also an interesting adsorbate because it is usually present under ambient conditions and therefore may influence catalytic processes on TiO_2 surfaces.[22] Furthermore, the substitution energies of surface hydroxyl groups with halide ions are calculated for all halides. Surface phase diagrams are derived from the DFT results to compare the stability of the competing surface and adsorption structures depending on the experimental conditions and the chemical environment. Access to the stabilization processes allows us to predict particle shapes via the Wulff construction. Finally, TiO_2 NPs are synthesized from different halide precursors (TiF_4, $TiCl_4$, $TiBr_4$, and TiI_4) in non-aqueous synthesis. The shapes and compositions of the synthesized particles are then analyzed by transmission electron microscopy (TEM), energy-dispersive x-ray spectroscopy (EDX), and x-ray powder diffraction (XRD) and compared to the computational results.

II. METHODS

A. Computational methods

Total energy calculations based on density functional theory (DFT) with a plane wave basis set were performed using the Vienna *Ab initio* Simulation Package (VASP).[23,24] The atomic core and the inner electrons were treated with the projector augmented-wave (PAW) method,[25] while the outer (valence) electrons were included explicitly in the calculations. Convergence with respect to cut-off energy, the number of k-points, the size of the vacuum region separating the periodic images, and the number of layers in the surface slab was tested for the different systems and reached with an accuracy of 1 meV/atom. All structures were relaxed to minimize the forces acting on the atoms to less than 5 meV/Å. Calculations on hydrohalic acid adsorption and substitution were performed using symmetric surface slabs with 10 layers of TiO_2, whereas asymmetric slabs with only 6 or 7 layers of TiO_2 were used to study carboxylic acid adsorption with reduced computational costs. Since van-der-Waals interactions cannot be neglected for the carboxylic acids,[26] the optB88-vdW exchange and correlation (XC) functional[27,28] was used for all calculations. A detailed comparison with the PBE (Perdew-Burke-Ernzershof) XC-functional[29] can be found in the supplementary material. The calculated adsorption structures using these different functionals are the same and deviate only in the picometer (10^{-12} m) range. The adsorption energies, however, are more negative for the optB88-vdW functional. Furthermore, van-der-Waals interactions increase with the size of the molecule and the size of the halide.

The adsorption energies per adsorbate molecule E_{ad} were calculated from

$$E_{ad} = \frac{1}{N}(E_{slab,ad} - E_{slab} - N \times E_{mol}), \quad (1)$$

where $E_{slab,ad}$, E_{slab}, and E_{mol} are the total energies of the adsorbates-on-slab structure, the clean surface slab, and the adsorbate molecule in a large vacuum cell, respectively, and N is the number of adsorbate molecules. Dissociative adsorption of acids on oxide surfaces produces hydroxyl groups on these surfaces. In hydrohalic acid environments, the substitution of hydroxyl groups by halide ions is studied. Since water is a byproduct of this process, the substitution energy is defined by

$$E_{sub} = \frac{1}{M}[E_{slab,sub} - E_{slab,ad} + M \times (E_{H_2O} - E_{mol})], \quad (2)$$

where $E_{slab,sub}$ and E_{H_2O} are the total energies of the substitution structure and the water molecule in a large vacuum cell, respectively, and M is the number of additional adsorbate molecules needed for a complete substitution of the first surface layer.

At 0 K and fixed volume, the surface free energies γ_0 of the stoichiometric TiO_2 surface slabs are given by

$$\gamma_0 = \frac{1}{A}\left(E_{\mathrm{slab,ad}} - N_{TiO_2} \times E_{TiO_2} - N \times E_{\mathrm{mol}}\right), \quad (3)$$

where A is the total surface area of the slab, E_{TiO_2} is the energy of one TiO_2 formula unit in the bulk, and N_{TiO_2} is the number of formula units of TiO_2 in the surface slab. Following the derivation by Reuter and Scheffler,[30] the surface free energy γ under experimental conditions, namely, finite temperature T and gas phase pressure p or solute concentration c, can be extrapolated from γ_0. In this approximation, the difference in the experimental state and the state at 0 K is completely attributed to the change in the chemical potential $\Delta\mu = \mu - E_{\mathrm{ad}}$ of the adsorbate,

$$\gamma = \gamma_0 + \frac{N}{A} \times \Delta\mu(T, c_{\mathrm{ad}}). \quad (4)$$

In the case of a substitution process as aforementioned, the change in the chemical potential of water $\Delta\mu_{H_2O} = \mu_{H_2O} - E_{H_2O}$ also has to be taken into account, resulting in

$$\gamma = \tilde{\gamma}_0 + \frac{(N+M)}{A} \times \Delta\mu(T, c_{\mathrm{ad}}) - \frac{M}{A} \times \Delta\mu_{H_2O}(T, c_{H_2O}), \quad (5)$$

where

$$\tilde{\gamma}_0 = \gamma_0 + \frac{M}{A} \times E_{\mathrm{sub}} \quad (6)$$

includes the effect of substitution at 0 K. The calculated surface free energies are then plotted vs the chemical potential change $\Delta\mu$ in surface phase diagrams to visualize the influence of different experimental conditions on the stability of the calculated structures. Because the solution for the non-aqueous synthesis in this work is highly complex and non-ideal, it is not possible to calculate an analytical expression for the function $\Delta\mu(T, c)$. Still, the surface phase diagrams can give valuable insight into how sensitively the system will react to a change under experimental conditions.

B. Materials

Titanium(IV) chloride ($TiCl_4$, 99%), titanium(IV) bromide ($TiBr_4$, 98%), 1-octadecene (ODE, 90%), oleic acid (OLAC, 90%), and 1-octadecanol (ODOL, 70%) were purchased from Sigma Aldrich. Titanium(IV) fluoride (TiF_4, 99%) and titanium(IV) iodide (TiI_4, 99.9%) were purchased from Alfa Aesar. Chloroform (99%), acetone (≥99.8%), and toluene (99.5%) were purchased from VWR. All chemicals were used as received without purification.

C. Synthesis of titania nanoparticles

The synthesis of TiO_2 nanoparticles was carried out via a non-aqueous seeded growth process introduced by Gordon *et al.*[11] All steps were carried out under the nitrogen atmosphere using standard Schlenk-line techniques. First, a solution of 8.0 g ODE, 8.09 g ODOL, and 0.51 ml OLAC (denoted as *growth solution* in the following) as well as a solution of 7.9 g ODE and 2.8 g OLAC (denoted as *precursor solution* in the following) were degassed under vacuum (10^{-2} mbar) at 120 °C for 1 h. Both solutions were allowed to cool down to 50 °C. Afterwards, 2.59 mmol of a titanium(IV)-halide precursor (TiF_4, $TiBr_4$, $TiCl_4$, and TiI_4) was added to the precursor solution and dissolved under stirring. Following continued stirring for at least 10 min after the complete dissolution of the precursor, 0.8 ml of the precursor solution was added to the growth solution under stirring. The growth solution was heated to 320 °C under constant stirring and kept at this temperature for 10 min. 4.5 ml of the precursor solution was added via a syringe pump (18 ml h^{-1}) while keeping the temperature constant. After continued stirring for 10 min, the reaction mixture was allowed to cool down to room temperature. By adding an equivalent volume of acetone to the solution, the nanoparticles were precipitated and separated from the solvents by centrifugation with at least 8000 × g. For purification, the precipitate was redispersed in chloroform and again precipitated by the addition of acetone followed by centrifugation. This purification procedure was repeated at least two times. Finally, the precipitate was redispersed in 15 ml–30 ml of chloroform.

X-ray powder diffraction (XRD) was used to characterize the crystal structure of the titania nanoparticles. After multiple washing steps (as described above), 400 µl was dropped onto a silicon (911) XRD substrate and investigated using a PANalytical X'PERT Pro diffractometer (copper anode, 45 kV, 40 mA, Bragg–Brentano geometry).

Scanning electron microscopy (SEM) was performed using a LEO-1550 Gemini (ZEISS) microscope. For these measurements, 50 µl of the titania nanoparticle solution was drop coated onto a silicon wafer with a native oxide layer (1 cm × 1 cm) and allowed to dry.

Transmission electron microscopy (TEM) was used to determine the size and shape of the titania nanoparticles. The titania nanoparticles were transferred as a diluted solution in toluene onto carbon coated copper grids and investigated using a Jeol JEM-1011 (LaB_6 cathode, 100 kV). Additionally, TEM-energy-dispersive x-ray spectroscopy (EDX) measurements were performed using a Jeol JEM 2200 FS (FEG cathode, 200 kV, Oxford X-Max 100TLE, SDD 100 mm^2). Here, the titania nanoparticles were precipitated again by the addition of acetone and subsequent centrifugation. The precipitate was redispersed in toluene. Afterward, a diluted nanoparticle solution (1:100) was transferred to carbon coated copper grids.

III. RESULTS AND DISCUSSION

The overall aim of this work is to obtain a comprehensive picture of the adsorption of hydrohalic and carboxylic acids on anatase TiO_2 surfaces in order to assess their influence on the shape of TiO_2 nanoparticles. A summary of the calculated adsorption and, if applicable, substitution energies can be found in Table I. In the following, the main computational results are highlighted, discussed, and then compared with the experimental results.

A. Hydrohalic and carboxylic acid adsorption

As shown in Table I, the adsorption energies per molecule of hydrohalic acids on anatase TiO_2 surfaces range from −1.11 eV to −1.43 eV. Here, they were calculated for a dissociative adsorption fully covering the surface as illustrated in Fig. 2.

TABLE I. Calculated adsorption and, if applicable, substitution energies per molecule in eV for hydrohalic and carboxylic acids on anatase TiO_2 (001), (100), and (101) surfaces for given coverages θ.

Species	θ	$E_{ad}(001)$	$E_{ad}(100)$	$E_{ad}(101)$	$E_{sub}(001)$	$E_{sub}(100)$	$E_{sub}(101)$
HF	1.0	−1.43	−1.33	−1.41	−0.40	−0.24	−0.11
HCl	1.0	−1.12	−1.11	−1.25	2.43	0.30	0.47
HBr	1.0	−1.19	−1.21	−1.36	1.83	0.60	0.77
HI	1.0	−1.12	−1.17	−1.34	1.06	1.11	1.19
Acetic acid	0.5	−1.91	−1.90	−1.61	...	...	...
Acetic acid	1.0	−1.43	−1.43	−1.50	...	...	...
Benzoic acid	0.5	−2.22	−2.16	−1.82	...	...	...
Benzoic acid	1.0	−0.48	−1.67	−1.79	...	...	...

Fluoric acid adsorbs stronger than the other hydrohalic acids and prefers the (001) surface. The other hydrohalic acids prefer the (101) surface and exhibit similar adsorption energies and structures among them (see the supplementary material for structures including Br and I). The equilibrium distance between the adsorbed fluoride anion and the surface (1.80 Å–1.88 Å) is slightly smaller than the Ti–O bond length of ≈2 Å, whereas the other adsorbed halide anions are further away from the surface (2.25 Å–2.95 Å).

Except for a full coverage adsorption of benzoic acid on the (001) surface, the carboxylic acids adsorb more strongly on the anatase TiO_2 surfaces than the hydrohalic acids. Excluding the full coverage adsorption of benzoic acid on the (001) surface, the adsorption energies range from −1.43 eV to −2.22 eV. Here, different adsorption modes (bidentate and monodentate, with and without dissociation) were studied, but only the results for the most stable ones are included in Table I. These most stable adsorption modes are shown for benzoic acid in Fig. 3. At half covered surfaces, the dissociative, bidentate adsorption at two neighboring Ti atoms is favored. However, this structure does not allow for a full coverage of the surface. Therefore, a pseudo-bidentate configuration with a Ti–O bond and a bridging hydrogen bond is preferred at full coverage. Acetic acid exhibits the same preferred adsorption modes (see the supplementary material), which agrees well with studies on formic acid adsorption on anatase TiO_2 surfaces.[31,32] The only major difference between benzoic acid and acetic acid appears at the (001) surface. Here, the density of adsorption sites is higher than that for the other surfaces. Therefore, neighboring benzoic acid adsorbates repel each other at full coverage, resulting in an increase in energy. For the smaller acetic acid, this effect is less pronounced, leading to a stronger adsorption than for benzoic acid in this case. It has to be noted that for the (001) surface, full coverage with benzoic acid is not observed experimentally,[33] which can be attributed to the low adsorption

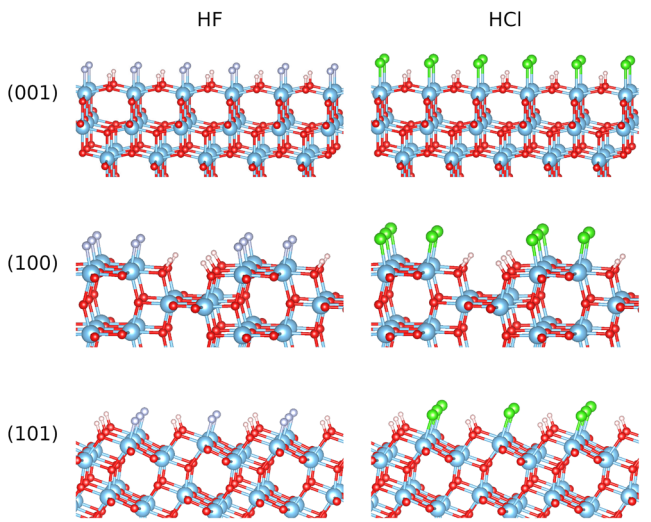

FIG. 2. Surface structures after hydrohalic acid adsorption. Top to bottom: (001), (100), and (101) surfaces of anatase TiO_2. Left: structures containing F. Right: structures containing Cl. Color code: Ti—blue, O—red, H—white, F—silver, and Cl—green.

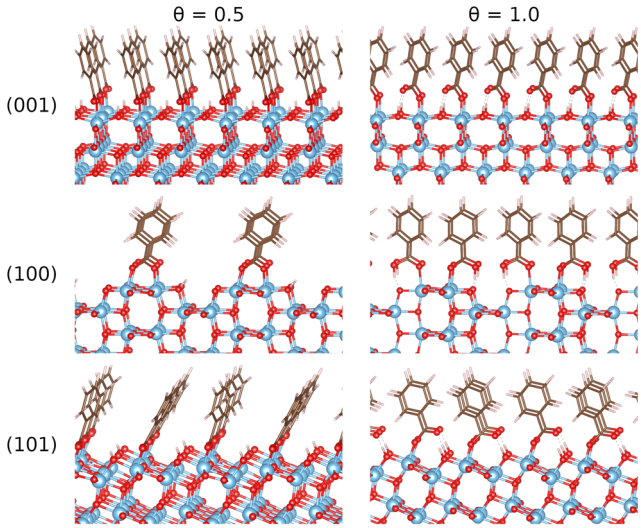

FIG. 3. Surface structures after benzoic acid adsorption. Top to bottom: (001), (100), and (101) surfaces of anatase TiO_2. Left: structures with a coverage θ of half a monolayer. Right: structures with full coverage θ. Color code: Ti—blue, O—red, C—brown, and H—white.

TABLE II. Calculated surface free energies in J m^{-2} at 0 K excluding (γ_0) and including ($\tilde{\gamma}_0$) the substitution process for hydrohalic and carboxylic acids adsorbed on anatase TiO_2 (001), (100), and (101) surfaces for given coverages θ.

Species	θ	$\gamma_0(001)$	$\gamma_0(100)$	$\gamma_0(101)$	$\tilde{\gamma}_0(001)$	$\tilde{\gamma}_0(100)$	$\tilde{\gamma}_0(101)$
None (cs)	0.0	0.92[a]	0.89	0.77	...	...	...
HF	1.0	−0.27	−0.26	−0.37	−0.71	−0.47	−0.46
HCl	1.0	0.07	−0.08	−0.23	2.75	0.19	0.14
HBr	1.0	0.00	−0.16	−0.33	2.02	0.36	0.29
HI	1.0	0.08	−0.12	−0.31	1.25	0.84	0.65
Acetic acid	0.5	0.25	0.06	0.11	...	...	...
Acetic acid	1.0	−0.28	−0.36	−0.45	...	...	...
Benzoic acid	0.5	0.08	−0.06	0.03	...	...	...
Benzoic acid	1.0	0.78	−0.57	−0.69	...	...	...

[a] 1×4 reconstruction.

energy and the corresponding higher surface energy (see Sec. III D, Table II). However, the adsorption structure at half coverage agrees well with the experimental and theoretical results from DeBenedetti *et al.*[33]

B. Hydroxyl ↔ halide substitution

Hydrogen stemming from the carboxylic and hydrohalic acids used during synthesis may bind to the oxygen at the surface of the TiO_2 nanoparticles forming surface hydroxyl groups (see Figs. 2 and 3). As shown in the sixth to eighth columns of Table I, the substitution of these surface hydroxyl groups by halide ions is energetically favorable only for fluoride. All the other substitution energies are positive and therefore unfavorable. Furthermore, the substitution process with fluoride or iodide favors the (001) surface, whereas for the other halides, the substitution energies are lowest on the (100) surface. The HF energies compare well with literature values by Wang *et al.*,[19] who first proposed this substitution process on the (101) and (001) surfaces and a corresponding selective etching process on the (001) surface.

The substitution structures for HF and HCl on the different TiO_2 surfaces are shown in Fig. 4. For HBr and HI, the structures are very similar to the HCl structures (see the supplementary material). The structures indicate that Cl^-, Br^-, and I^- ions are too large to substitute the hydroxyl group at the surface of TiO_2. Therefore, they relax outwards, repelling the halide adsorbed on the surface Ti atom. This increases the energy of the system resulting in a positive substitution energy. The increase in substitution energies with ion size in Table I for the (100) and (101) surfaces further supports this explanation. The inversed order of the substitution energies on the (001) surface can be explained by the tensile stress present in the clean, unreconstructed (001) surface.[21] Here, larger ions lead to a stronger release of the tensile stress and therefore to lower substitution energies. Fluoride anions substituting hydroxyl groups at the surface, on the other hand, are small enough to relax inwards. Thereby, the Coulomb attraction toward the neighboring Ti^{4+} cations is maximized and tensile stresses are reduced, which results in negative substitution energies.

C. Lifting of the (001) 1 × 4 reconstruction

The (001) surface of anatase TiO_2 shows a 1×4 reconstruction in ultra-high vacuum, because of the tensile stress in the unreconstructed 1×1 structure.[21] The stress is reduced in the reconstructed structure by an additional TiO_2 ridge (see Fig. 5), which reduces the free surface energy of the clean surface from 1.31 J m^{-2} to 0.92 J m^{-2}. On this ridge, the adsorption energies of all hydrohalic acids are more negative (−1.19 eV to −1.59 eV) than on the unreconstructed 1×1 surface. On the plateau between the ridges, however, the adsorption energies are more positive (−0.53 eV to −0.76 eV). Therefore, at coverages larger than one molecule per 1×4 unit cell, hydrohalic acids bind stronger to the unreconstructed surface than to the reconstructed 1×4 surface.

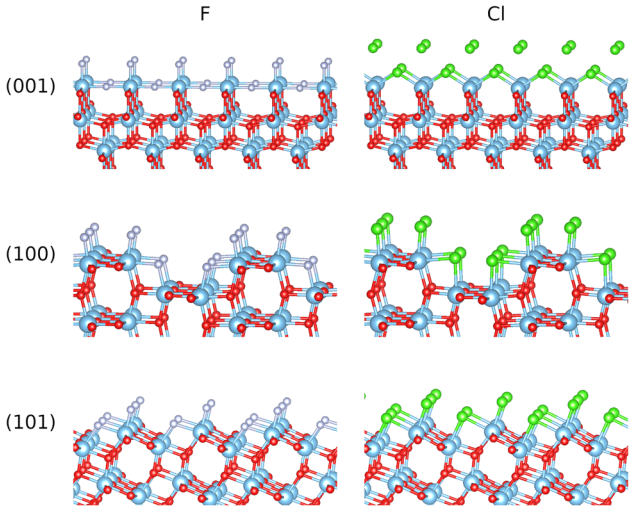

FIG. 4. Surface structures after the hydroxyl ↔ halide substitution process. Top to bottom: (001), (100), and (101) surfaces of anatase TiO_2. Left: structures containing F. Right: structures containing Cl. Color code: Ti—blue, O—red, F—silver, and Cl—green.

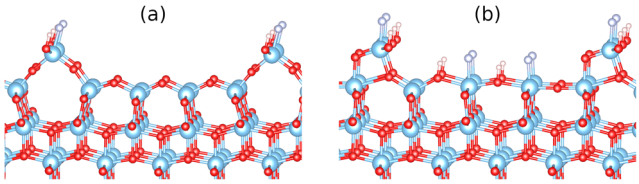

FIG. 5. Structure of the 1 × 4 reconstructed (001) surface after adsorption of 1 HF molecule on the ridge (a) and 3 HF molecules on the ridge and plateau (b). Color code: Ti—blue, O—red, F—silver, and H—white.

Looking at the relaxed surface structure at a higher coverage of HF in Fig. 5(b), one can see that the surface tends to go back to the unreconstructed structure. The ridge can then be seen as an adsorbed TiO_2–HF molecule. Similar structures are observed for the other hydrohalic acids. Contrary to another computational study on HF adsorption at the (001) surface of anatase TiO_2,[34] here, the free surface energy of the reconstructed surface with a full coverage of HF is higher than the free surface energy of the unreconstructed surface with a full coverage of HF. The difference of the findings may be due to the different functionals and computational settings used. On the other hand, in accordance with the results presented here, a combined experimental and theoretical study found that the reconstruction is not the thermodynamic ground state in benzoic acid and HF aqueous solutions and only formed at temperatures above 550 °C.[33] Furthermore, the aforementioned substitution of surface hydroxyl groups by halide ions also releases the tensile stress on the unreconstructed (001) surface. Since this eliminates the driving force for the reconstruction, the substitution process will also lift the reconstruction. Hence, the {001} facets of synthesized anatase TiO_2 particles will not be reconstructed.

D. Insights from surface phase diagrams

Following Eqs. (3) and (6), the free surface energies at 0 K of the structures described above were calculated. As made apparent in Table II, many of the calculated surface free energies are negative. This means that the associated process of creating the corresponding surface structure is thermodynamically favorable and occurs spontaneously. Often this is interpreted as leading to a dissolution of the particle because more and more surface is created until there is no bulk structure left. This interpretation, however, is only valid for clean surface structures. For adsorption structures, the creation of new surfaces with the same structure also involves the adsorbate molecule. Therefore, the creation of new surfaces can only happen through intermediate structures. These are usually less favorable and hence act as an energetic barrier for the dissolution of the particle. Only for fluoric acid, an etching process on the {001} facets with favorable intermediate structures is known in the literature.[19]

In order to assess the stability of the different surface structures under varying experimental conditions, surface phase diagrams are created and displayed in Figs. 6 and 7. They depict the most stable facet–adsorbate combination at different chemical potentials of the corresponding molecules. Therefore, they can give insight into competitive adsorption processes and the shape of anatase TiO_2 nanoparticles. As there are many possible combinations, the discussion here is restricted to diagrams shown in Figs. 6 and 7, which are most important for understanding the aqueous and non-aqueous synthesis of TiO_2 nanoparticles. Additional phase diagrams are shown in the supplementary material.

The phase diagram for fluoric and chloric acid adsorption and substitution in Fig. 6 clearly shows that the substitution structures become more stable when the water chemical potential is reduced. Therefore, surfaces where the hydroxyl groups are substituted by halide ions are more stable in non-aqueous synthesis of TiO_2 nanoparticles than in aqueous synthesis. Furthermore, for a high HCl chemical potential, the {100} facets are stabilized through substitution, whereas HF stabilizes the {001} facets. This suggests an alternative explanation for the cuboid shaped particles observed in mixtures of HCl and HF, which exhibit only {001} and {100} facets.[18,20] Instead of the face selective substitution of adsorbed chloride by fluoride proposed by Wu *et al.*,[18] our calculations show that the cuboid structure is stabilized thermodynamically by the substitution of surface hydroxyl groups by chloride.

Surface phase diagrams can also give valuable insight into understanding competitive adsorption processes. Figure 7 shows the

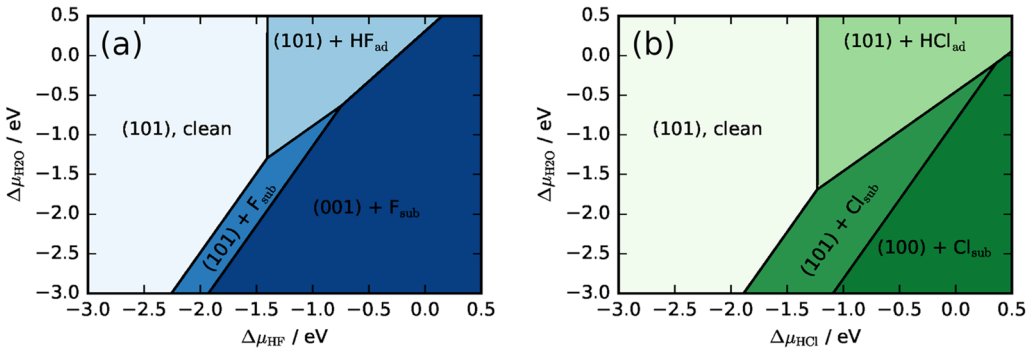

FIG. 6. Surface phase diagrams of anatase TiO_2 surfaces in hydrohalic acid environment. Influence of fluoric acid and water chemical potential (a) and chloric acid and water chemical potential (b) on the stability of the {001}, {100}, and {101} facets.

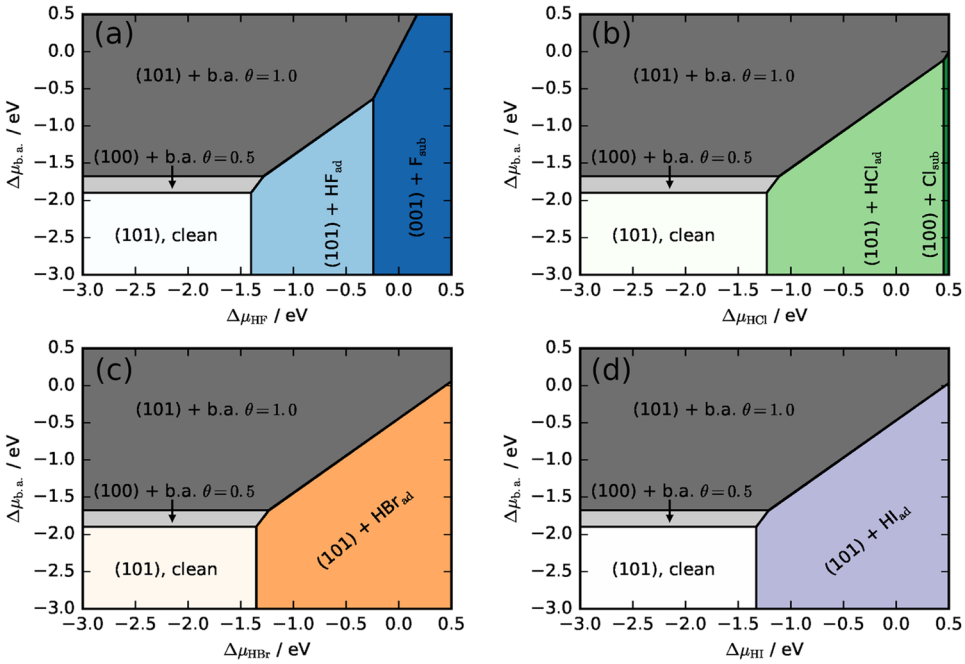

FIG. 7. Surface phase diagrams of anatase TiO_2 surfaces in carboxylic and hydrohalic acid environment. Influence of benzoic acid (b.a.) and (a) fluoric acid, (b) chloric acid, (c) bromic acid, and (d) iodic acid on the stability of the {001}, {100}, and {101} facets. For the substitution structures, the water chemical potential shift $\Delta\mu_{H_2O}$ was fixed to 0 eV.

calculated surface phase diagrams for the competitive adsorption of carboxylic and hydrohalic acids on anatase TiO_2 nanoparticle surfaces. Since benzoic acid is closer to the oleic acid used in experiments, the results for this molecule are shown here. The surface phase diagrams for acetic acid are also very similar, as can be seen in the supplementary material. Interestingly, at half coverage of benzoic acid, the {100} facet is most stable, whereas at full coverage, the {101} facet is most stable. This may cause the particle shape to change, depending on the carboxylic acid concentration from rod or cuboid shaped particles to bipyramidal particles. On the other hand, the stability range for the half covered surface is at very low chemical potential. Therefore, it may be difficult to stabilize this phase. Comparing the diagrams for different halides in Fig. 7, similar trends are observed for Cl, Br, and I. These three halides stabilize the {101} facet and can be replaced easily with carboxylic acids such as benzoic acid because even for the high chemical potential of the corresponding hydrohalic acid, the carboxylic acid structures are usually more stable. The surface phase diagram including F [Fig. 7(a)], on the other hand, has a different appearance. The favorable substitution of hydroxyl groups stabilizes the {001} facet at higher HF chemical potentials. This does not only cause platelet-shaped nanoparticles with a larger area of {001} facets but may also block the adsorption sites for carboxylic acids impeding the functionalization with these ligands.

E. Shape and composition of synthesized nanoparticles

The titania nanoparticles of this study were synthesized using a procedure based on the non-aqueous synthesis reported by Gordon *et al.*[11] Here, OLAC is required as an oxygen source. OLAC also forms an oleate complex with the titanium(IV) ions in the precursor solution. After addition to the growth solution and heating to 320 °C, titania seeds are formed. Further addition of the precursor leads to continued growth of these seeds. Depending on the type of halides present as well as the type of organic ligands, different nanoparticle shapes and crystal structures are formed.[10,11] Figure 8 shows the TEM micrographs of TiO_2 nanoparticles

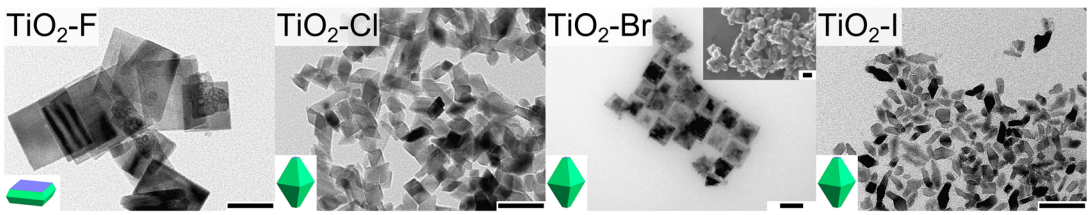

FIG. 8. TEM micrographs for nanoparticles synthesized using different titanium(IV) halides. The inset for TiO_2–Br shows an SEM micrograph to better illustrate the 3D shape of the nanoparticles (scale bar: 50 nm).

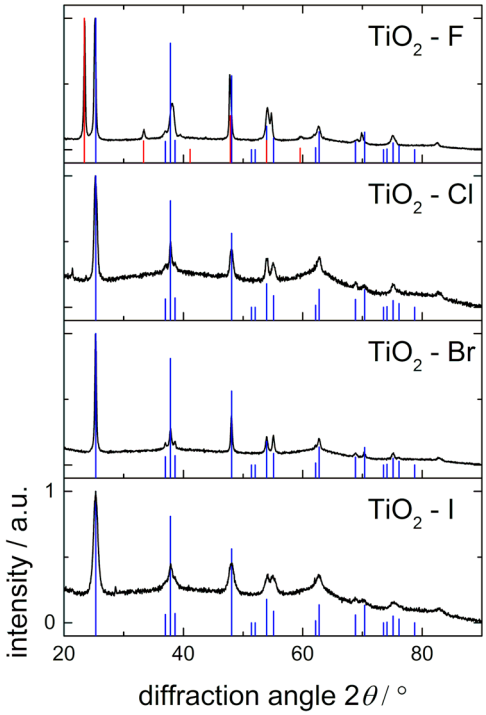

FIG. 9. XRD data of nanoparticle samples synthesized using different titanium(IV) halide precursors. Reference diffractograms for anatase (blue, ICSD collection code: 9852) and $TiOF_2$ (red, ICSD collection code: 160661) are shown.

synthesized using the four different titanium(IV) halide precursors. It is to note that the reaction temperature of 320 °C used in our study was higher than in the protocol of Gordon *et al.* (290 °C).[11] This increase in temperature was necessary to enable the formation of TiO_2 nanocrystals when using the TiI_4 precursor. In order to maintain comparable reaction conditions, we adjusted the increased reaction temperature also for the syntheses using the other precursors.

As shown in the literature[12] and confirmed by the calculations above, the presence of fluoride ions leads to plate-like growth of titania nanoparticles (TiO_2–F). Presumably, the low degree of stabilization of the {101} facets by the ODOL ligands leads to comparatively large platelets[11] with an edge length of up to about 70 nm. In the presence of chloride ions, nanoparticles with a bipyramidal shape and an average size of about 30 nm are formed (TiO_2–Cl). As predicted by the computational results, the shapes of the nanoparticles synthesized in the presence of bromide (TiO_2–Br) and iodide ions (TiO_2–I) are similar to TiO_2–Cl. For TiO_2–Br nanoparticles, the size is increased up to approximately 60 nm. Due to the pronounced edge-to-edge assembly of the nanoparticles shown in the TEM micrograph (Fig. 8), the bipyramidal shape is not clearly visible, but was confirmed via SEM (see the inset in the TEM micrograph and the supplementary material). Additionally, a more step-like pyramidal structure of the nanoparticles is observed. This may be caused by the low formation energy of step edges on TiO_2 (101) in general,[35] but further studies are needed to provide insights into the interactions of these defects with halides. For iodide ions (TiO_2–I), the nanoparticles' shape is less defined compared to TiO_2–Cl. The TiO_2–I nanoparticles are smaller with an average size of about 20 nm and have a somewhat more elongated shape. Nevertheless, the similarity to the bipyramidal shape of the TiO_2–Cl sample is clearly visible.

Investigation of the crystal phases utilizing XRD (see Fig. 9) revealed that the crystal phase for the TiO_2–Cl, TiO_2–Br, and TiO_2–I nanoparticles is anatase. In the case of the TiO_2–F nanoparticles, $TiOF_2$ is formed besides the TiO_2 anatase phase. TEM micrographs show that the majority of nanoparticles have a plate-like shape, as previously reported by Gordon *et al.*[11] However, another nanoparticle species with a less defined shape is also observed. High resolution TEM micrographs reveal that the plate-like nanoparticles exhibit lattice plane distances of 0.35 nm, which is the characteristic distance of the {101} lattice planes in anatase. In the other nanoparticle species, this lattice plane distance is absent and, instead, a lattice plane distance of 0.38 nm is observed, which is the characteristic

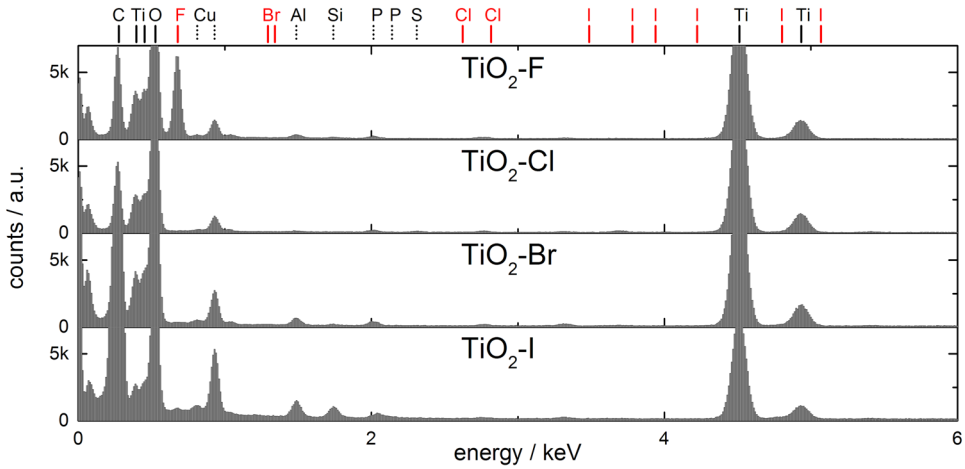

FIG. 10. EDX analysis of nanoparticles synthesized using the different titanium(IV) halide precursors. The lines indicate the expected elements (Ti, O, black solid lines), determined contaminations (black dotted lines), and the halides (red solid lines).

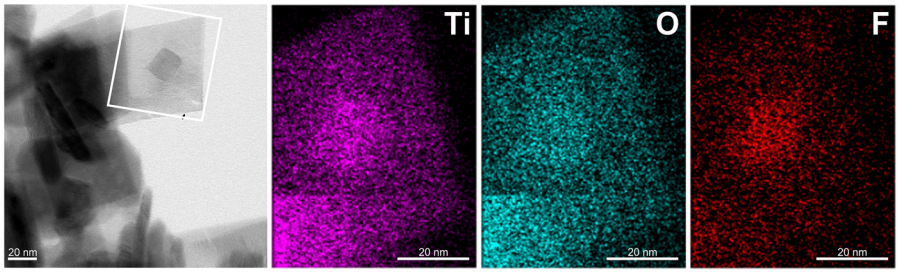

FIG. 11. EDX mapping data for isolated TiO_2–F nanoparticles synthesized using titanium(IV) fluoride. Within the area marked in the SEM micrograph (left), the signals of titanium (Ti, violet), oxygen (O, teal), and fluorine (F, red) are shown.

distance of the {100} lattice planes in $TiOF_2$ (see the supplementary material). Thus, the anatase XRD pattern observed for the TiO_2–F sample could clearly be assigned to the plate-like nanoparticles. Furthermore, it is to note that reducing the reaction temperature to 290 °C for the synthesis of TiO_2–F nanoparticles produces almost exclusively anatase nanoplates, in agreement with the literature.[11] In this case, only faint signals of $TiOF_2$ could be observed in the XRD data (see the supplementary material).

The elemental composition of the nanoparticles was characterized by EDX. A high amount of fluorine could be detected for the TiO_2–F sample, in addition to the expected titanium and oxygen content as shown in Fig. 10. Figure 11 shows EDX mapping data measured from isolated TiO_2–F nanoplates. The signals of the individual elements (Ti, O, and F) are distributed over the entire nanoparticle. Previously, Gordon *et al.* characterized titania nanoplates via x-ray photoelectron spectroscopy.[11] Their data suggest that fluorine binds to Ti on the nanoparticle surface. However, the high ratio of fluorine to titanium of ≈0.8 observed by EDX in single anatase nanoparticles indicates that fluorine may have additionally been incorporated into the lattice structure during nanoparticle growth. For the other precursors ($TiCl_4$, $TiBr_4$, and TiI_4), no signal corresponding to the used halides could be detected by EDX (Fig. 10). Thus, in agreement with the theoretical data, the binding/incorporation of these halides to/into formed anatase nanoparticles is much less pronounced than in the case of the TiO_2–F sample.

IV. CONCLUSION

In this paper, the influence of different chemical environments on the shape of anatase TiO_2 nanoparticles was studied with a combination of *ab initio* surface science and experimental techniques. For fluoric acid, the well-known stabilization of the {001} facet resulting in platelet-shaped particles was observed. As described in the literature, the reason for this stabilization is the substitution of surface hydroxyl groups by fluoride, which was confirmed here through XRD and EDX measurements. The substitution of surface hydroxyl groups by other halides, however, was found to be energetically unfavorable under typical synthesis conditions. EDX and XRD measurements confirmed this computational result, finding no evidence of remaining halides in the synthesized particles. Furthermore, chloric, bromic, and iodic acid adsorption did not change the energetic ordering of the different facets of anatase TiO_2 nanoparticles. Particles synthesized in these environments have the typical bipyramidal shape of clean anatase TiO_2 particles. The non-aqueous synthesis of TiO_2 nanoparticles is usually performed with carboxylic acids as reactants. Therefore, competitive adsorption of hydrohalic and carboxylic acids was also studied here using acetic and benzoic acid as representatives of the latter group. Chloric, bromic, and iodic acid are found to adsorb weaker than the carboxylic acids, so the resulting particles are covered with carboxylic acid. Fluoric acid, on the other hand, adsorbs more strongly and is still present after synthesis, possibly blocking adsorption sites.

SUPPLEMENTARY MATERIAL

See the supplementary material for a comparison of the optB88-vdW and PBE XC functionals, additional structures for HBr, HI, and acetic acid adsorption, additional substitution structures including Br and I, additional surface phase diagrams including Br, I, and acetic acid, a SEM micrograph showing NPs synthesized using titanium(IV) bromide, a Fast Fourier Transformation (FFT) analysis of high-resolution TEM micrographs of TiO_2–F NPs, and a TEM micrograph and XRD data for TiO_2–F NPs synthesized at 290 °C.

ACKNOWLEDGMENTS

This work was funded by the Deutsche Forschungsgemeinschaft (DFG, German Research Foundation)—Project No. 192346071—SFB 986.

The authors thank Robert Schön and Stefan Werner for SEM and TEM measurements, Andreas Kornowski for TEM and EDX measurements, and Almut Barck for XRD measurements.

REFERENCES

[1] X. Chen and S. S. Mao, "Titanium dioxide Nanomaterials: Synthesis, properties, modifications, and applications," Chem. Rev. **107**, 2891–2959 (2007).

[2] A. Fujishima, X. Zhang, and D. A. Tryk, "TiO_2 photocatalysis and related surface phenomena," Surf. Sci. Rep. **63**, 515–582 (2008).

[3] X. Chen, S. Shen, L. Guo, and S. S. Mao, "Semiconductor-based photocatalytic hydrogen generation," Chem. Rev. **110**, 6503–6570 (2010).

[4] L. DeRita, J. Resasco, S. Dai, A. Boubnov, H. V. Thang, A. S. Hoffman, I. Ro, G. W. Graham, S. R. Bare, G. Pacchioni, X. Pan, and P. Christopher, "Structural evolution of atomically dispersed Pt catalysts dictates reactivity," Nat. Mater. **18**, 746 (2019).

[5] B. K. Roy, G. Zhang, and J. Cho, "Titanium oxide nanoparticles precipitated from low-temperature aqueous solutions: III. Thin film properties," J. Am. Ceram. Soc. **95**, 676–683 (2012).

[6]F. Liaqat, M. N. Tahir, E. Schechtel, M. Kappl, G. K. Auernhammer, K. Char, R. Zentel, H.-J. Butt, and W. Tremel, "High-performance TiO_2 nanoparticle/DOPA-polymer composites," Macromol. Rapid Commun. **36**, 1129–1137 (2015).
[7]A. Hensel, C. J. Schröter, H. Schlicke, N. Schulz, S. Riekeberg, H. K. Trieu, A. Stierle, H. Noei, H. Weller, and T. Vossmeyer, "Elasticity of cross-linked titania nanocrystal assemblies probed by AFM-bulge tests," Nanomaterials **9**, 1230 (2019).
[8]P. D. Cozzoli, A. Kornowski, and H. Weller, "Low-temperature synthesis of soluble and processable organic-capped anatase TiO_2 nanorods," J. Am. Chem. Soc. **125**, 14539–14548 (2003).
[9]J. Joo, S. G. Kwon, T. Yu, M. Cho, J. Lee, J. Yoon, and T. Hyeon, "Large-scale synthesis of TiO_2 nanorods via nonhydrolytic sol-gel ester elimination reaction and their application to photocatalytic inactivation of *E. coli*," J. Phys. Chem. B **109**, 15297–15302 (2005).
[10]R. Buonsanti, V. Grillo, E. Carlino, C. Giannini, T. Kipp, R. Cingolani, and P. D. Cozzoli, "Nonhydrolytic synthesis of high-quality anisotropically shaped brookite TiO_2 nanocrystals," J. Am. Chem. Soc. **130**, 11223–11233 (2008).
[11]T. R. Gordon, M. Cargnello, T. Paik, F. Mangolini, R. T. Weber, P. Fornasiero, and C. B. Murray, "Nonaqueous synthesis of TiO_2 nanocrystals using TiF_4 to engineer morphology, oxygen vacancy concentration, and photocatalytic activity," J. Am. Chem. Soc. **134**, 6751–6761 (2012).
[12]M.-H. Yang, P.-C. Chen, M.-C. Tsai, T.-T. Chen, I.-C. Chang, H.-T. Chiu, and C.-Y. Lee, "Alkali metal ion assisted synthesis of faceted anatase TiO_2," CrystEngComm **15**, 2966–2971 (2013).
[13]U. Diebold, "The surface science of titanium dioxide," Surf. Sci. Rep. **48**, 53–229 (2003).
[14]M. Lazzeri, A. Vittadini, and A. Selloni, "Structure and energetics of stoichiometric TiO_2 anatase surfaces," Phys. Rev. B **63**, 155409 (2001).
[15]M. R. Ranade, A. Navrotsky, H. Z. Zhang, J. F. Banfield, S. H. Elder, A. Zaban, P. H. Borse, S. K. Kulkarni, G. S. Doran, and H. J. Whitfield, "Energetics of nanocrystalline TiO_2," Proc. Natl. Acad. Sci. U. S. A. **99**, 6476–6481 (2002).
[16]A. S. Barnard and L. A. Curtiss, "Prediction of TiO_2 nanoparticle phase and shape transitions controlled by surface chemistry," Nano Lett. **5**, 1261–1266 (2005).
[17]H. G. Yang, C. H. Sun, S. Z. Qiao, J. Zou, G. Liu, S. C. Smith, H. M. Cheng, and G. Q. Lu, "Anatase TiO_2 single crystals with a large percentage of reactive facets," Nature **453**, 638–641 (2008).
[18]L. Wu, B. X. Yang, X. H. Yang, Z. G. Chen, Z. Li, H. J. Zhao, X. Q. Gong, and H. G. Yang, "On the synergistic effect of hydrohalic acids in the shape-controlled synthesis of anatase TiO_2 single crystals," CrystEngComm **15**, 3252–3255 (2013).
[19]Y. Wang, H. Zhang, Y. Han, P. Liu, X. Yao, and H. Zhao, "A selective etching phenomenon on {001} faceted anatase titanium dioxide single crystal surfaces by hydrofluoric acid," Chem. Commun. **47**, 2829–2831 (2011).
[20]Z. Lai, F. Peng, Y. Wang, H. Wang, H. Yu, P. Liu, and H. Zhao, "Low temperature solvothermal synthesis of anatase TiO_2 single crystals with wholly {100} and {001} faceted surfaces," J. Mater. Chem. **22**, 23906–23912 (2012).
[21]M. Lazzeri and A. Selloni, "Stress-driven reconstruction of an oxide surface: The anatase $TiO_2(001) - (1 \times 4)$ surface," Phys. Rev. Lett. **87**, 266105 (2001).
[22]J. Balajka, M. A. Hines, W. J. I. DeBenedetti, M. Komora, J. Pavelec, M. Schmid, and U. Diebold, "High-affinity adsorption leads to molecularly ordered interfaces on TiO_2 in air and solution," Science **361**, 786–789 (2018).
[23]G. Kresse and J. Furthmüller, "Efficient iterative schemes for *ab initio* total-energy calculations using a plane-wave basis set," Phys. Rev. B **54**, 11169–11186 (1996).
[24]G. Kresse and J. Furthmüller, "Efficiency of ab-initio total energy calculations for metals and semiconductors using a plane-wave basis set," Comput. Mater. Sci. **6**, 15–50 (1996).
[25]P. E. Blöchl, "Projector augmented-wave method," Phys. Rev. B **50**, 17953–17979 (1994).
[26]W. Heckel, T. Würger, S. Müller, and G. Feldbauer, "Van der Waals interaction really matters: Energetics of benzoic acid on TiO_2 rutile surfaces," J. Phys. Chem. C **121**, 17207–17214 (2017).
[27]J. Klimeš, D. R. Bowler, and A. Michaelides, "Chemical accuracy for the van der Waals density functional," J. Phys.: Condens. Matter **22**, 022201 (2010).
[28]J. Klimeš, D. R. Bowler, and A. Michaelides, "Van der Waals density functionals applied to solids," Phys. Rev. B **83**, 195131 (2011).
[29]J. P. Perdew, K. Burke, and M. Ernzerhof, "Generalized gradient approximation made simple," Phys. Rev. Lett. **77**, 3865–3868 (1996).
[30]K. Reuter and M. Scheffler, "Composition, structure, and stability of $RuO_2(110)$ as a function of oxygen pressure," Phys. Rev. B **65**, 035406 (2001).
[31]A. Vittadini, A. Selloni, F. P. Rotzinger, and M. Grätzel, "Formic acid adsorption on dry and hydrated TiO_2 anatase (101) surfaces by DFT calculations," J. Phys. Chem. B **104**, 1300–1306 (2000).
[32]X.-Q. Gong, A. Selloni, and A. Vittadini, "Density functional theory study of formic acid adsorption on anatase $TiO_2(001)$: Geometries, energetics, and effects of coverage, hydration, and reconstruction," J. Phys. Chem. B **110**, 2804–2811 (2006).
[33]W. J. I. DeBenedetti, E. S. Skibinski, D. Jing, A. Song, and M. A. Hines, "Atomic-scale understanding of catalyst activation: Carboxylic acid solutions, but not the acid itself, increase the reactivity of anatase (001) faceted nanocatalysts," J. Phys. Chem. C **122**, 4307–4314 (2018).
[34]S. Selçuk and A. Selloni, "Surface structure and reactivity of anatase TiO_2 crystals with dominant {001} facets," J. Phys. Chem. C **117**, 6358–6362 (2013).
[35]X.-Q. Gong, A. Selloni, M. Batzill, and U. Diebold, "Steps on anatase TiO_2 (101)," Nat. Mater. **5**, 665–670 (2006).